Supporting information

for

Porphodilactones as Synthetic Chlorophylls: Relative Orientation of β-Substituents On a Pyrrolic Ring Tunes NIR Absorption

Xian-Sheng Ke,[†] Yi Chang,[‡] Jia-Zhen Chen,[†] Jiangwei Tian,[‡] John Mack,[§] Xin Cheng,[†] Zhen Shen*,[‡] and Jun-Long Zhang*,[†]

[†]Beijing National Laboratory for Molecular Sciences, State Key Laboratory of Rare Earth Materials Chemistry and Applications, College of Chemistry and Molecular Engineering, Peking University, Beijing 100871, P.R. China.

[‡]State Key Laboratory of Coordination Chemistry, School of Chemistry and Chemical Engineering, Nanjing University, Nanjing 210093 P.R. China.

[§]Department of Chemistry, Rhodes University, Grahamstown 6140, South Africa.

Table of Contents

1. Supporting information for synthesis and characterization S4

1.1. Figure S1. Opposite forms and adjacent forms of porphodilactones proposed by Gouterman and co-workers. S4

1.2. Approaches to isolate ***trans-*** and ***cis*-H_2F_{20}TPPDL** free bases S5

1.2.1. Figure S2. UV-visible absorption spectra (Q band) changes. (a) recrystallization process; (b) Soxhlet extraction S5

1.2.2. Figure S3. HPLC analysis of mixture of two isomers. (DCM (0.1%TEA)/n-Hexane gradient) S6

1.2.3. Figure S4. HPLC analysis of mixture of two isomers. (H_2O/CH_3CN gradient) S7

1.2.4. Figure S5. Supercritical Fluid Chromatography of the mixture of two isomers. (supercritical fluid (CO_2) with 8% isopropanol) S8

1.3. Detailed procedure for isolation of metalloporphodilactones S9

1.3.1. Figure S6. UV-visible absorption spectra changes during the silica gel chromatography process for (a) Ni(II) complexes and (b) Zn(II) complexes. S9

1.4. Table S1. Crystal data and structure refinement for *trans*-Zn(py_2)F_{20}TPPDL S10

1.5. Table S2. Crystal data and structure refinement for *cis*-Zn(py_2)F_{20}TPPDL S11

1.6. Table S3. Photophysical properties of porphodilactones in DCM. S12

1.7. Figure S7. Normalized excitation (monitored at 678 nm) and emission (excited at 410 nm) spectra of ***trans*-H_2F_{20}TPPDL** in DCM at $3x10^{-7}$M. S13

1.8. Figure S8. Normalized excitation (monitored at 662 nm) and emission (excited at 408 nm) spectra of ***cis*-H_2F_{20}TPPDL** in DCM at $3x10^{-7}$M. S14

1.9. Figure S9. Normalized excitation (monitored at 666nm) and emission (excited at 410 nm) spectra of ***trans*-ZnF_{20}TPPDL** in DCM at $3x10^{-7}$M. S15

1.10. Figure S10. Normalized excitation (monitored at 644nm) and emission (excited at 423nm) spectra of ***cis*-ZnF_{20}TPPDL** in DCM at $3x10^{-7}$M. S16

1.11. Figure S11. Cyclic voltammograms of the porphodilactones in DCM containing 0.1 M NBu_4PF_6. (V *vs* SCE). S17

2. Supporting information for singlet oxygen quantum yield determination and cell experiment. S18

2.1. Figure S12. Changes in the absorption spectra of DPBF upon irradiation (λ_{irr} = 635nm) with 60s interval in the presence of (a) H_2F_{20}TPPL and (b) methylene blue (MB). S18

2.2. Figure S13. Changes in the absorption spectra of DPBF upon irradiation (λ_{irr} = 671nm) with 10s interval in the presence of (a) ***trans*-H_2F_{20}TPPDL**, (b) ***trans*-ZnF_{20}TPPDL** and (c) methylene blue (MB). S19

2.3. Figure S14. Changes in the absorption spectra of DPBF upon irradiation (λ_{irr}= 635nm) with 20s interval in the presence of (a) ***cis*-H_2F_{20}TPPDL**, (b) ***cis*-ZnF_{20}TPPDL** and (c) methylene blue (MB). S20

2.4. Figure S15. $^1O_2$ production from a plot of changes in absorbance by DPBF at 411 nm against irradiation time (λ_{irr} = 635 nm) in the presence of H_2F_{20}TPPL in CH_2Cl_2 *vs* MB (blue) as a standard. S21

2.5. Figure S16. $^1O_2$ production from a plot of changes in absorbance by DPBF at 411 nm against irradiation time (λ_{irr} = 671 nm) in the presence of ***trans*-H_2F_{20}TPPDL** or ***trans*-ZnF_{20}TPPDL** in CH_2Cl_2 *vs* MB (blue) as a standard. S22

2.6. Figure S17. $^1O_2$ production from a plot of changes in absorbance by DPBF at 411 nm against irradiation time (λ_{irr} = 635 nm) in the presence of ***cis*-ZnF_{20}TPPDL** in CH_2Cl_2 *vs* MB (blue) as a standard. S23

2.7. Figure S18. Confocal fluorescence images of propidium iodide (PI) stained HeLa cells with different treatments. (a) no treatment; (b) 60 μg·mL^{-1} ***trans*-ZnF$_{20}$TPPDL** loaded PLGA NPs incubation without irradiation; (c) irradiation without ***trans*-ZnF$_{20}$TPPDL** loaded PLGA NPs incubation; (d) 60 μg·mL^{-1} ***trans*-ZnF$_{20}$TPPDL** loaded PLGA NPs incubation combined with irradiation. S24

3. Supporting information for theoretical calculations S25

3.1 Table S4. The number of the excited state in ascending energy (#), calculated wavelengths (λ_{calc}) and oscillator strengths (f_{calc}), observed wavelengths of the Faraday $\mathcal{B}_0$ terms in the MCD spectra (λ_{obs}), oscillator strengths calculated from the experimental spectra (f_{obs}) through spectral band decovolution with the SIMPFIT program[a] of both spectra with Gaussian-shaped bands, and wavefunctions for H_2F_{20}TPP, H_2F_{20}TPPL, ***cis*-** and ***trans*-H$_2$F$_{20}$TPPDL**, ZnF_{20}TPP, ZnF_{20}TPPL, and ***cis*-** and ***trans*-ZnF$_{20}$TPPDL** S25

3.2. The complete reference of Gaussian 09 ..... S26

4. ^{1}H-, ^{19}F-, ^{13}C-NMR, IR and HR-ESI MS spectra S27

4.1. Figure S19. ^{1}H NMR spectrum of ***trans*-H$_2$F$_{20}$TPPDL** in $CDCl_3$.(400MHz) S27

4.2. Figure S20. ^{1}H NMR spectrum of ***cis*-H$_2$F$_{20}$TPPDL** in $CDCl_3$. (400MHz) S28

4.3. Figure S21. ^{1}H NMR spectrum of ***trans*-ZnF$_{20}$TPPDL** in $CDCl_3$. (400MHz) S29

4.4. Figure S22. ^{1}H NMR spectrum of ***cis*-ZnF$_{20}$TPPDL** in $CDCl_3$. (400MHz) S30

4.5. Figure S23. ^{19}F NMR spectrum of ***trans*-H$_2$F$_{20}$TPPDL** in $CDCl_3$. (471MHz) S31

4.6. Figure S24. ^{19}F NMR spectrum of ***cis*-H$_2$F$_{20}$TPPDL** in $CDCl_3$. (471MHz) S32

4.7. Figure S25. ^{19}F NMR spectrum of ***trans*-ZnF$_{20}$TPPDL** in $CDCl_3$. (471MHz) S33

4.8. Figure S26. ^{19}F NMR spectrum of ***cis*-ZnF$_{20}$TPPDL** in $CDCl_3$. (471MHz) S34

4.9. Figure S27. ^{13}C NMR spectrum of ***trans*-H$_2$F$_{20}$TPPDL** in $CDCl_3$. (126MHz) S35

4.10. Figure S28. ^{13}C NMR spectrum of ***cis*-H$_2$F$_{20}$TPPDL** in $CDCl_3$. (126MHz) S36

4.11. Figure S29. ^{13}C NMR spectrum of ***trans*-ZnF$_{20}$TPPDL** in $CDCl_3$. (126MHz) S37

4.12. Figure S30. ^{13}C NMR spectrum of ***cis*-ZnF$_{20}$TPPDL** in $CDCl_3$. (126MHz) S38

4.13. Figure S31. Normalized FI-IR spectra of ***trans*-H$_2$F$_{20}$TPPDL**. S39

4.14. Figure S32. Normalized FI-IR spectra of ***cis*-H$_2$F$_{20}$TPPDL**. S40

4.15. Figure S33. Normalized FI-IR spectra of ***trans*-ZnF$_{20}$TPPDL**. S41

4.16. Figure S34. Normalized FI-IR spectra of ***cis*-ZnF$_{20}$TPPDL**. S42

4.17. Figure S35. HR ESI-MS spectra and simulated results of porphodilactones. S43

1. Supporting information for synthesis and characterization

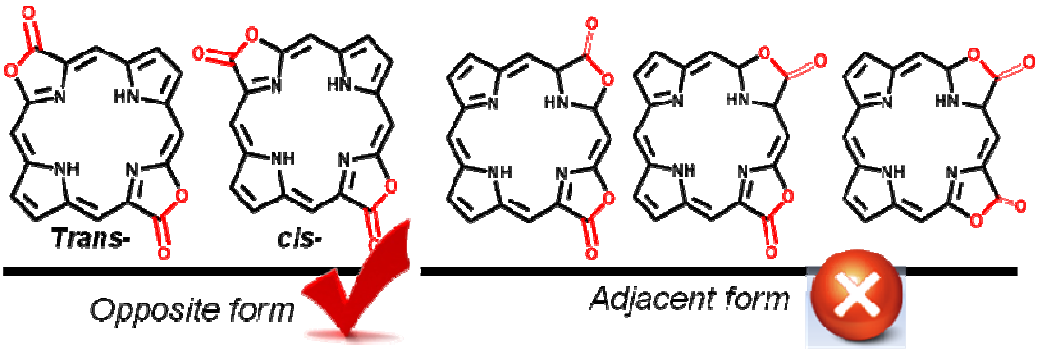

1.1. Figure S1. Opposite forms and adjacent forms of porphodilactones proposed by Gouterman and co-workers.

1.2. Approaches to isolate *trans*- and *cis*-H_2F_{20}TPPDL free bases

a) Crystallization: We tried to separate these two isomers by re-crystallization. In a typical run, 20 mg mixture (*trans*: *cis* = 3:2) was dissolved in 1 mL DCM in a centrifugal tube, then 10 mL hexane was added to the solution. After precipitation and centrifugation, *trans* isomer can be accumulated in the precipitation. The precipitation was used as starting material for the next recrystallization run. By repeating this process for 5 times, *trans*: *cis*=4:1 isomer mixture can be achieved (Figure S2a).

b) Soxhlet extraction: In this process, due to the nature that *cis* isomer has better solubility in hexane, *trans* isomer can be accumulated in the solid. However, we cannot get the pure *trans* isomer by this way, either. After 6 days' extraction, the solid obtained was a mixture of *trans*: *cis* = 19:1, and the yield is very low (~2%) (Figure S2b).

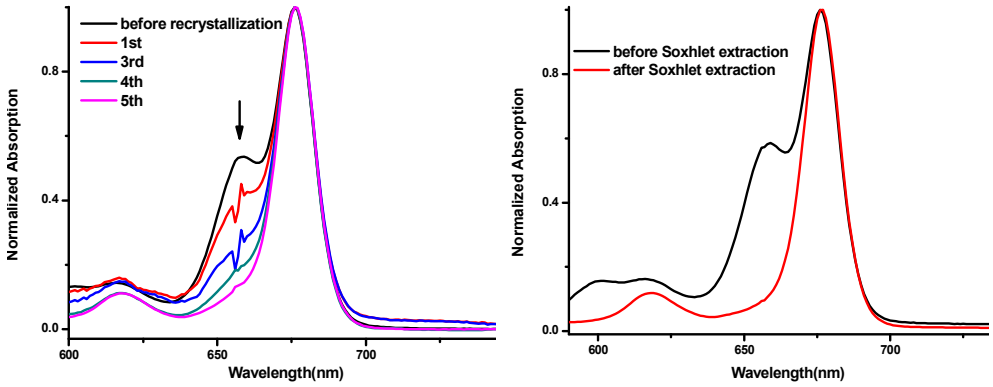

(a) (b)

1.2.1. Figure S2. UV-visible absorption spectra (Q band) changes. (a) recrystallization process; (b) Soxhlet extraction

c) HPLC chromatograph: Normal phase HPLC was performed firstly and different eluent such as DCM (0.1% TEA), DCM(0.1% TEA)/MeOH and DCM(0.1% TEA)/*n*-Hexane were used, only one peak was observed in all the condition above. The mixture still showed one peak when reverse phase HPLC was performed by using H_2O:CH_3CN as eluent. The two isomers could be isolated at analytical column by using Supercritical Fluid Chromatography (SFC), but failed at preparative column (10 mg scale).

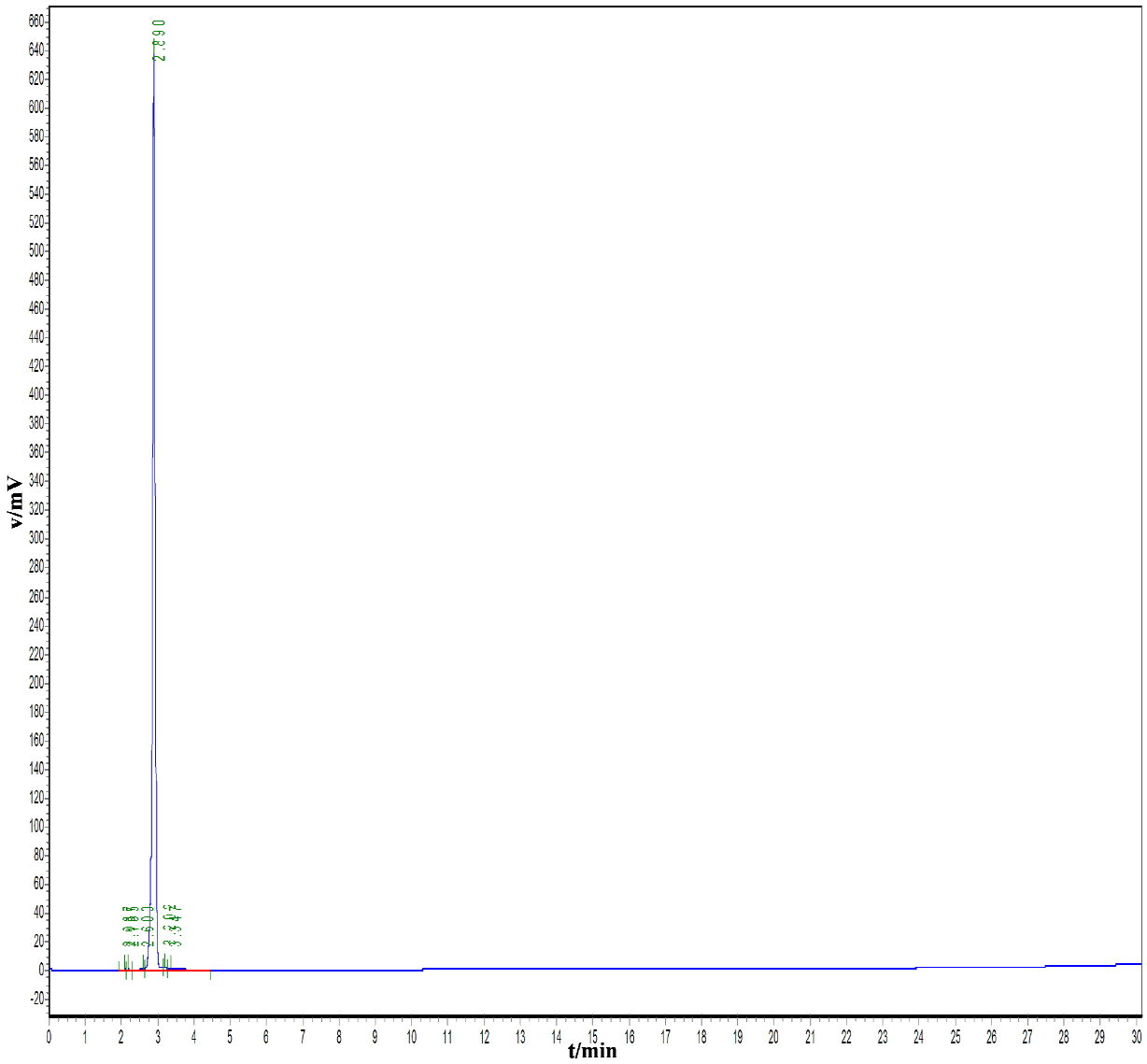

1.2.2. Figure S3. HPLC analysis of mixture of two isomers. (DCM (0.1%TEA)/n-Hexane gradient)

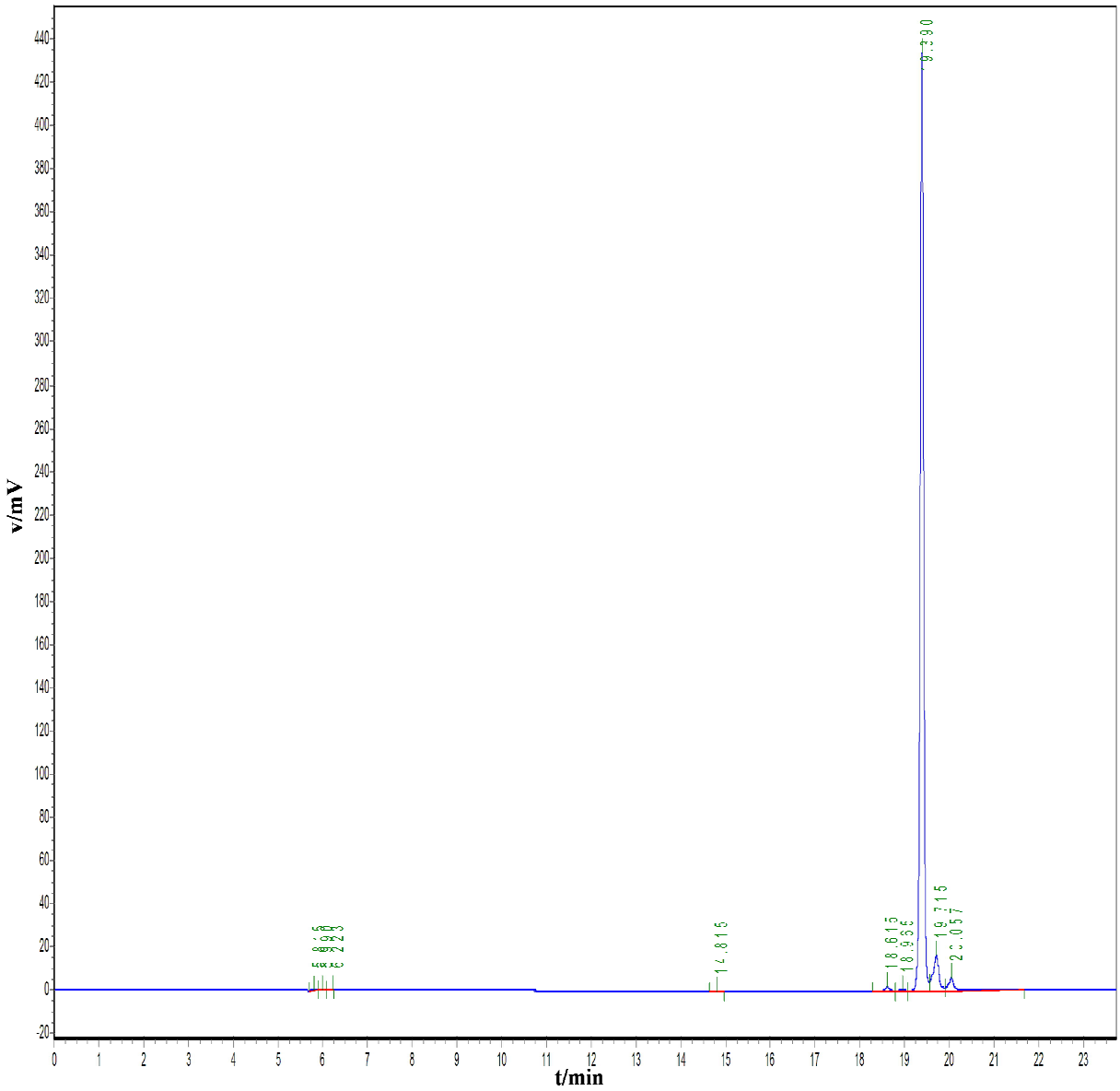

1.2.3. Figure S4. HPLC analysis of mixture of two isomers. (H_2O/CH_3CN gradient)

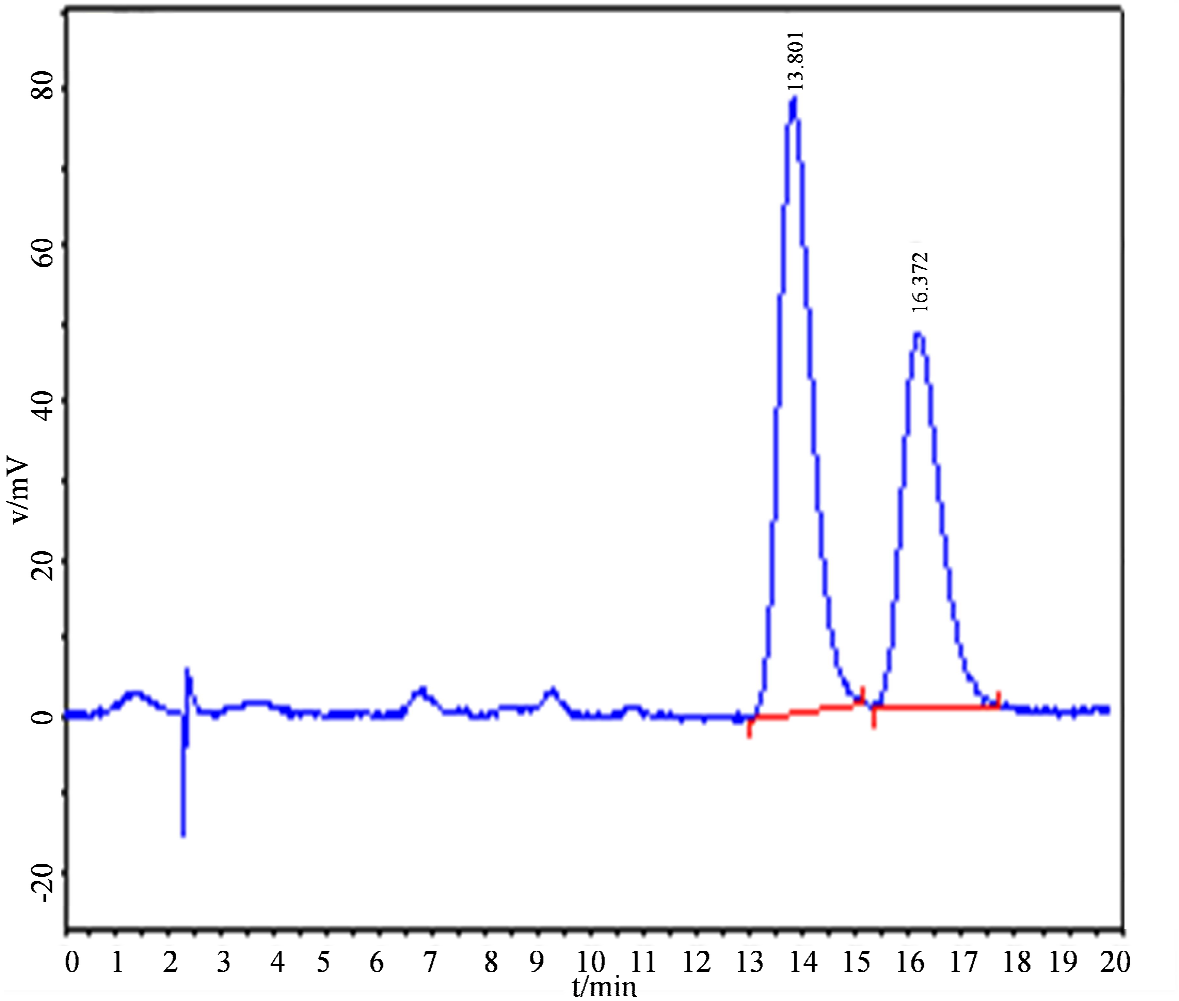

1.2.4. Figure S5. Supercritical Fluid Chromatography of the mixture of two isomers. (supercritical fluid (CO_2) with 8% isopropanol)

1.3. Detailed procedure for isolation of metalloporphodilactones

We metalized the isomers with Ni(II) and Zn(II) by refluxing the mixture of free ligands with metal salts in ethanol. Then, silica gel chromatography was performed respectively. For Ni(II) complexes, the first eluate was a mixture of two isomers with the *trans* isomer as the major component; the *cis* isomer became the major component as the chromatography process progressed and no pure isomer was obtained throughout the whole process (Figure S6a). For the Zn(II) complexes, surprisingly, the first eluate was found to be pure *trans* isomer (the isolation yield was 18%), while the isolation of the *cis* isomer was more difficult. The *cis* isomer was obtained in a yield of 8% after conducting the chromatography process three times (Figure S6b).

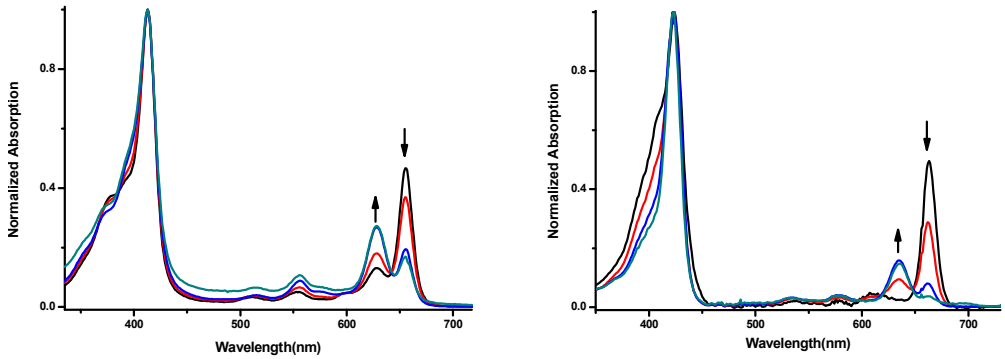

1.3.1. Figure S6. UV-visible absorption spectra changes during the silica gel chromatography process for (a) Ni(II) complexes and (b) Zn(II) complexes.

1.4. Table S1. Crystal data and structure refinement for *trans*-Zn(py_2)F_{20}TPPDL

Identification code	*trans*-Zn(py_2)F_{20}TPPDL
Empirical formula	C52.50 H18 F20 N6 O5.50 Zn
Formula weight	1266.10
Temperature/K	153(2)
Crystal system	triclinic
Space group	P-1
a/Å	11.871(2)
b/Å	13.856(3)
c/Å	17.697(4)
α/°	100.09(3)
β/°	107.95(3)
γ/°	97.64(3)
Volume/$Å^3$	2671.5(9)
Z	2
ρ_{calc}mg/mm^3	1.574
m/mm^{-1}	0.06
F(000)	1258
Crystal size/mm^3	0.06 × 0.05 × 0.01
2Θ range for data collection	2.18 to 25.00°
Index ranges	$0 \leq h \leq 14$, $-16 \leq k \leq 16$, $-21 \leq l \leq 19$
Reflections collected	8345
Independent reflections	7487[R(int) = 0.0365]
Data/restraints/parameters	8453/6/837
Goodness-of-fit on F^2	1.110
Final R indexes [I>=2σ (I)]	R_1 = 0.0721, wR_2 = 0.2162
Final R indexes [all data]	R_1 = 0.0672, wR_2 = 0.2108

1.5. Table S2. Crystal data and structure refinement for *cis*-Zn(py_2)F_{20}TPPDL

Identification code	*cis*-Zn(py_2)F_{20}TPPDL
Empirical formula	C49.50 H11.50 F20 N6 O4 Zn
Formula weight	1199.52
Temperature/K	179.98(16)
Crystal system	Monoclinic
Space group	C2/c
a/Å	14.8972(6)
b/Å	16.7644(8)
c/Å	37.8928(16)
α/°	90.00
β/°	91.327(4)
γ/°	90.00
Volume/$Å^3$	9460.9(7)
Z	8
ρ_{calc}mg/mm^3	1.562
m/mm^{-1}	0.02
F(000)	4740
Crystal size/mm^3	0.11 × 0.1 × 0.02
2Θ range for data collection	3.23 to 28.48°
Index ranges	$-18 \leq h \leq 15$, $-21 \leq k \leq 20$, $-47 \leq l \leq 50$
Reflections collected	10106
Independent reflections	6983 [R(int) = 0.0370]
Data/restraints/parameters	10106/1/760
Goodness-of-fit on F^2	1.054
Final R indexes [I>=2σ (I)]	R_1 = 0.0802, wR_2 = 0.2278
Final R indexes [all data]	R_1 = 0.1126, wR_2 = 0.2552

1.6. Table S3. Photophysical properties of porphodilactones in DCM.

Compound	Absorption λ_{max} [nm](lgε[$M^{-1}cm^{-1}$])	Excitation λ_{max} [nm]	Emission λ_{max} [nm](τ [ns])	Φ[a]
***trans*-H_2F_{20}TPPDL**	410(5.56), 512(4.15), 552(4.38), 676(4.89)	409	678(3.49),755	0.10
***cis*-H_2F_{20}TPPDL**	391(5.11), 408(5.62), 505(4.26), 657(4.47)	408	662(3.49), 711	0.090
***trans*-H_2F_{20}TPPDL**	425(5.37), 538(3.81), 610(4.09), 663(5.12)	424	666(0.65),740	0.025
***cis*-H_2F_{20}TPPDL**	425(5.53), 534(3.98), 580(4.10), 635(4.71)	426	644(0.81), 701	0.028

[a]The quantum yield standard used in this study was TPP in toluene (Φ = 0.10) for free base and ZnTPP in toluene (Φ = 0.033) for Zn complexes.

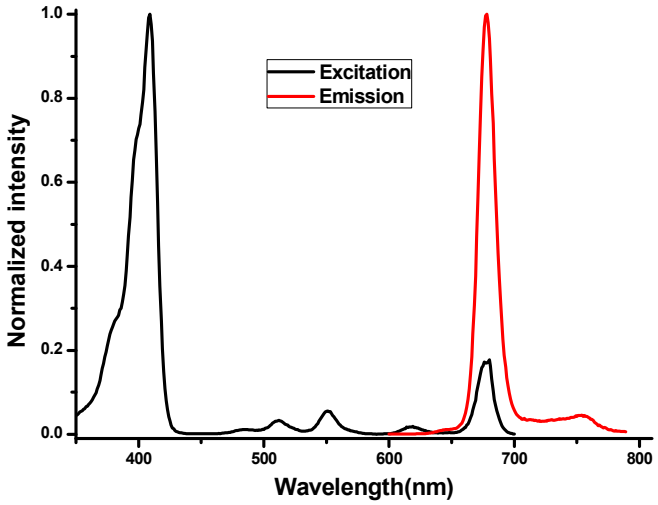

1.7. Figure S7. Normalized excitation (monitored at 678 nm) and emission (excited at 410 nm) spectra of ***trans*-H_2F_{20}TPPDL** in DCM at $3x10^{-7}$M.

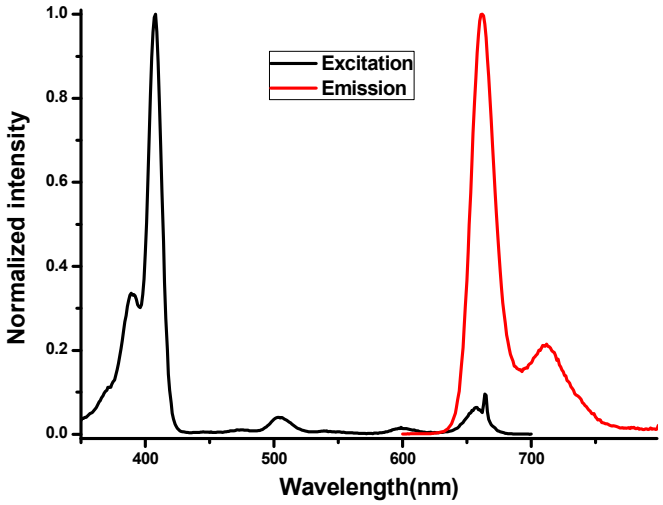

1.8. Figure S8. Normalized excitation (monitored at 662 nm) and emission (excited at 408 nm) spectra of ***cis*-H_2F_{20}TPPDL** in DCM at $3x10^{-7}$M.

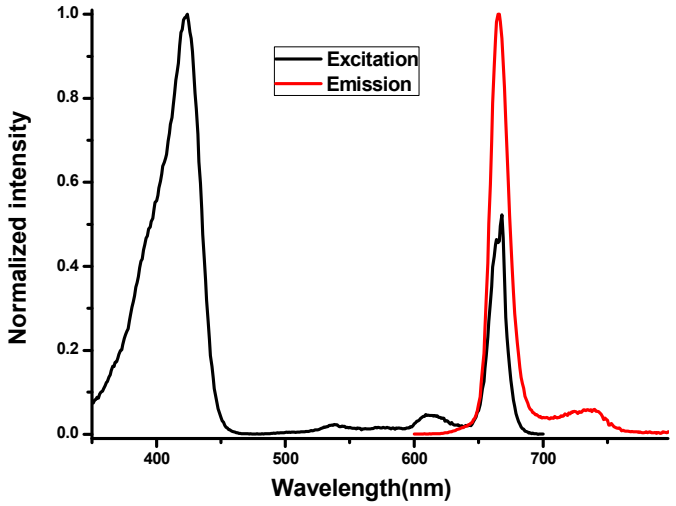

1.9. Figure S9. Normalized excitation (monitored at 666nm) and emission (excited at 410 nm) spectra of ***trans*-ZnF$_{20}$TPPDL** in DCM at 3x10^{-7}M.

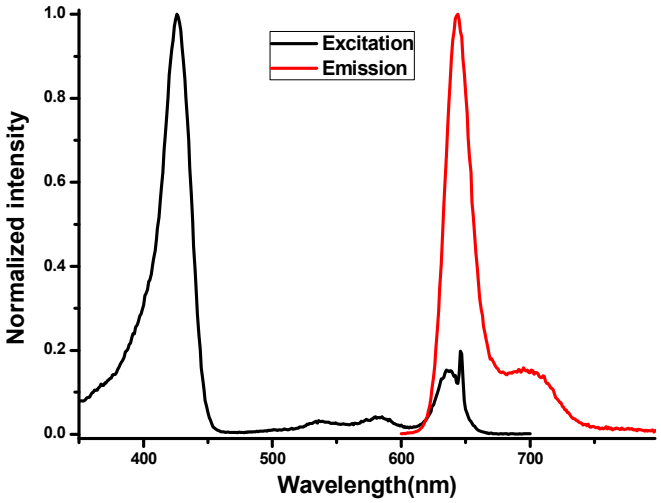

1.10. Figure S10. Normalized excitation (monitored at 644nm) and emission (excited at 423nm) spectra of ***cis*-ZnF$_{20}$TPPDL** in DCM at 3x10^{-7}M.

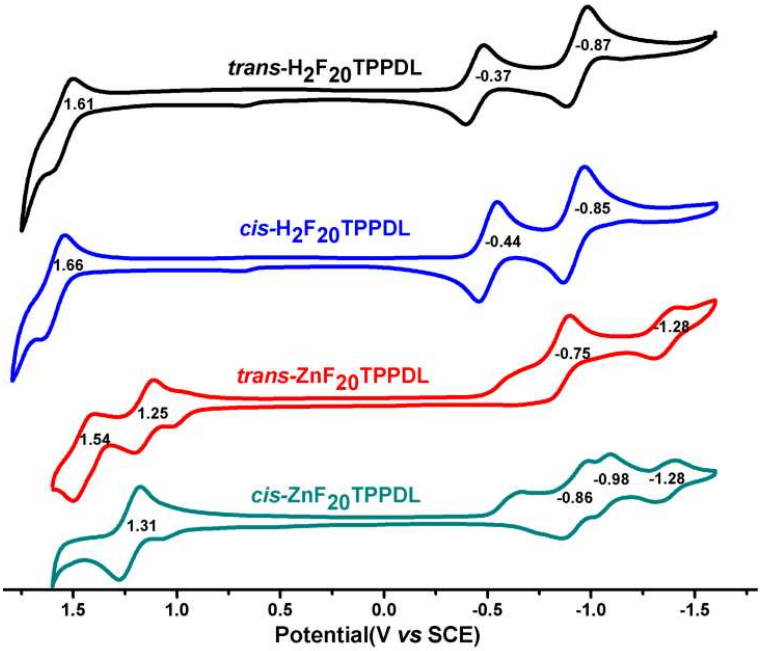

1.11. Figure S11. Cyclic voltammograms of the porphodilactones in DCM containing 0.1 M NBu_4PF_6. (V *vs* SCE).

2. Supporting information for singlet oxygen quantum yield determination and cell experiment.

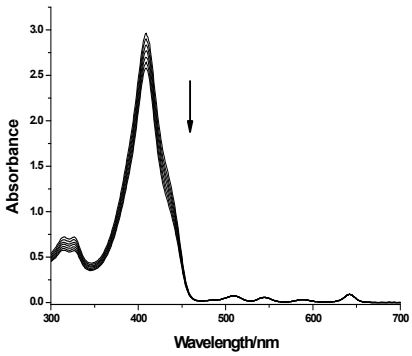

(a)

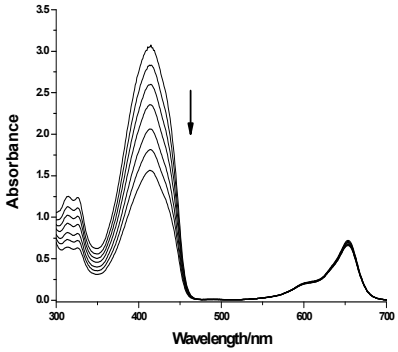

(b)

2.1. Figure S12. Changes in the absorption spectra of DPBF upon irradiation (λ_{irr} = 635nm) with 60s interval in the presence of (a) $H_2F_{20}TPPL$ and (b) methylene blue (MB).

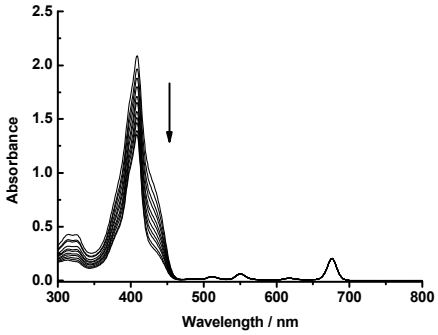

(a)

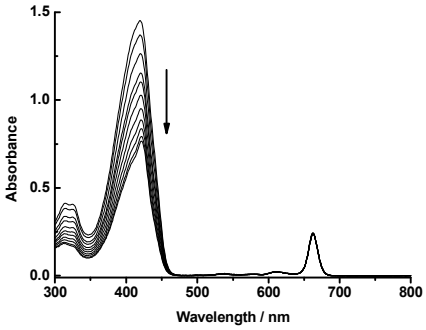

(b)

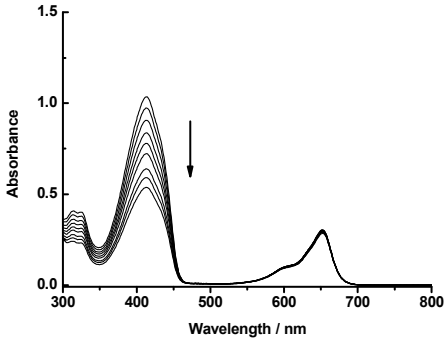

(c)

2.2. Figure S13. Changes in the absorption spectra of DPBF upon irradiation (λ_{irr} = 671nm) with 10s interval in the presence of (a) ***trans*-H_2F_{20}TPPDL**, (b) ***trans*-ZnF_{20}TPPDL** and (c) methylene blue (MB).

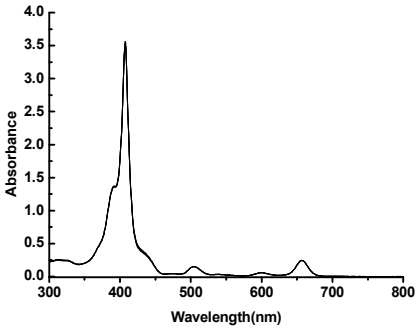

(a)

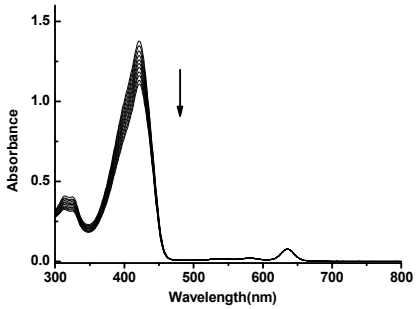

(b)

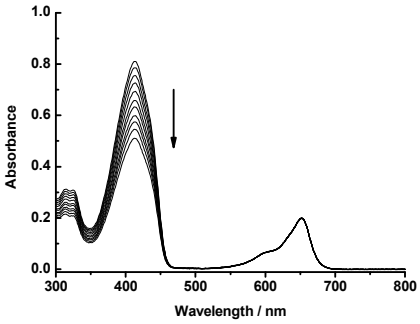

(c)

2.3. Figure S14. Changes in the absorption spectra of DPBF upon irradiation (λ_{irr}= 635nm) with 20s interval in the presence of (a) ***cis*-H_2F_{20}TPPDL**, (b) ***cis*-ZnF_{20}TPPDL** and (c) methylene blue (MB).

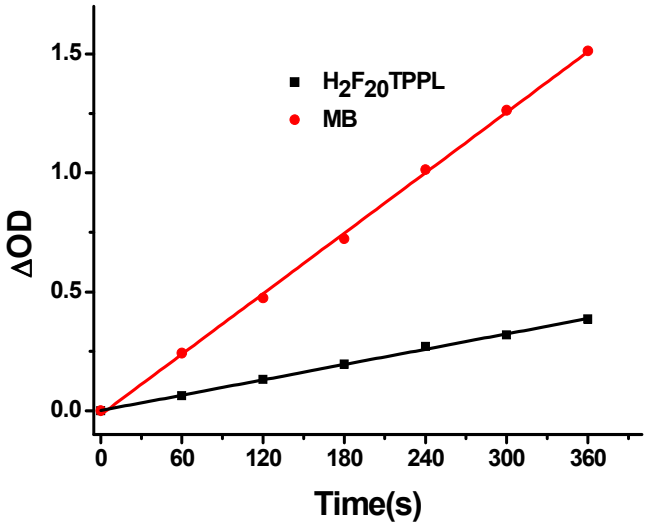

2.4. Figure S15. $^1O_2$ production from a plot of changes in absorbance by DPBF at 411 nm against irradiation time (λ_{irr} = 635 nm) in the presence of $H_2F_{20}TPPL$ in CH_2Cl_2 *vs* MB (blue) as a standard.

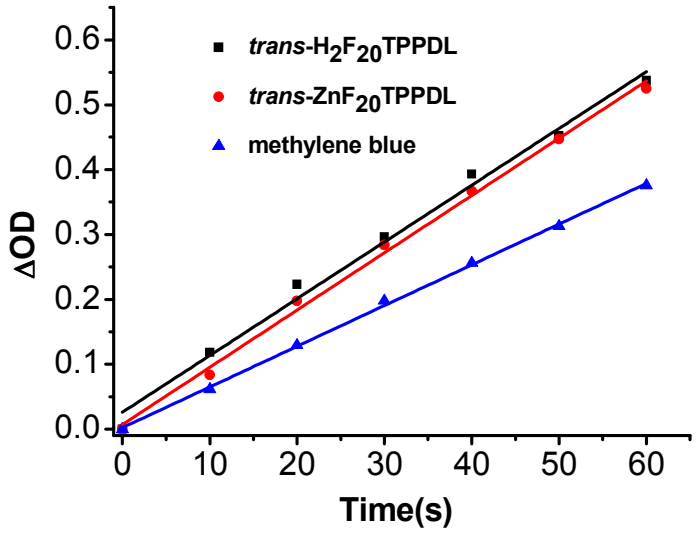

2.5. Figure S16. $^1O_2$ production from a plot of changes in absorbance by DPBF at 411 nm against irradiation time (λ_{irr} = 671 nm) in the presence of ***trans*-H_2F_{20}TPPDL** or ***trans*-ZnF_{20}TPPDL** in CH_2Cl_2 *vs* MB (blue) as a standard.

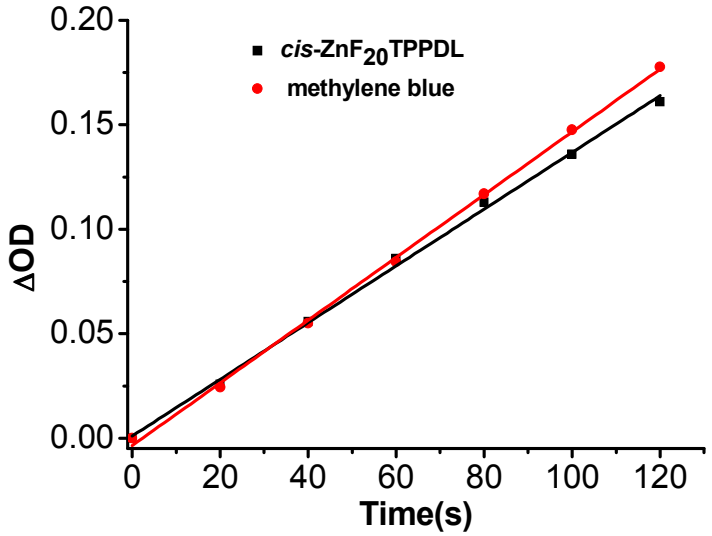

2.6. Figure S17. $^1O_2$ production from a plot of changes in absorbance by DPBF at 411 nm against irradiation time (λ_{irr} = 635 nm) in the presence of ***cis*-ZnF$_{20}$TPPDL** in CH_2Cl_2 *vs* MB (blue) as a standard.

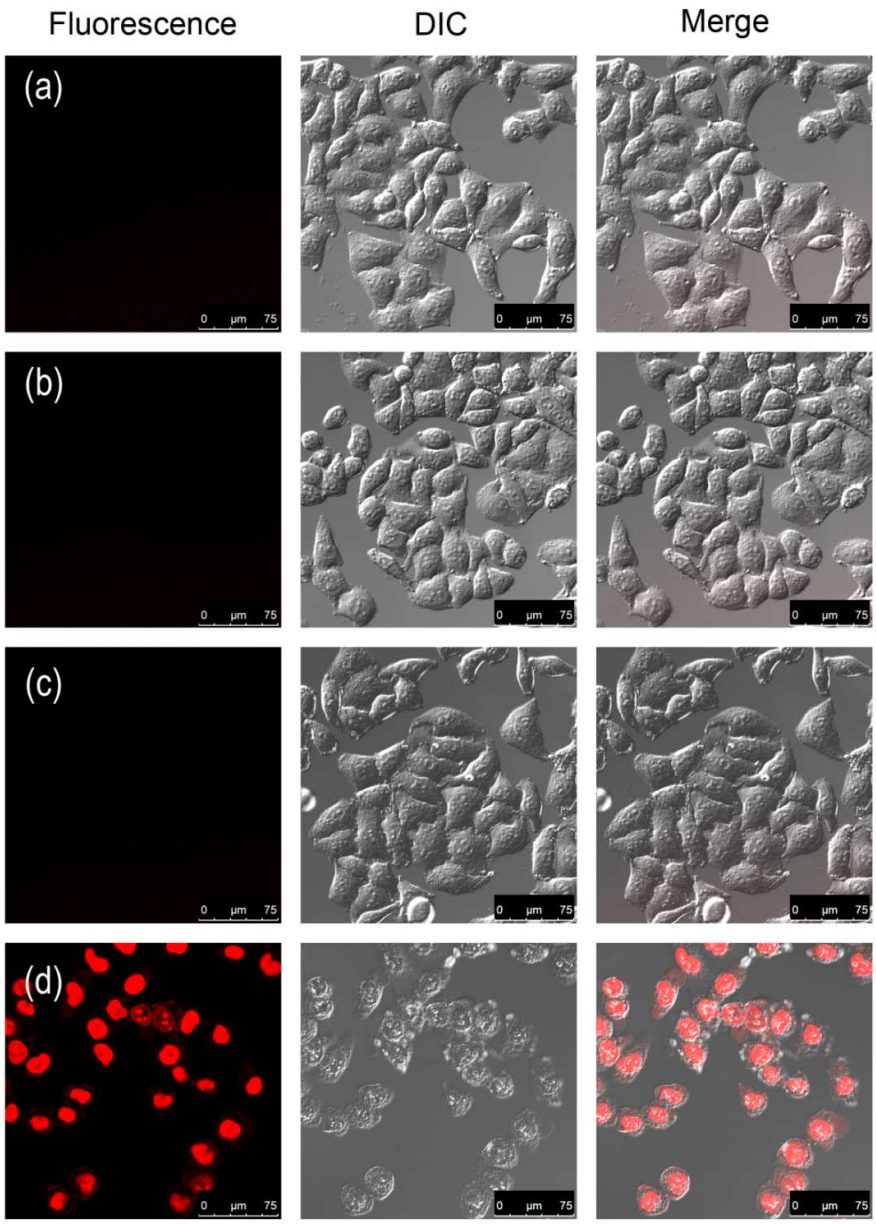

2.7. Figure S18. Confocal fluorescence images of propidium iodide (PI) stained HeLa cells with different treatments. (a) no treatment; (b) 60 μg·ml^{-1} ***trans*-ZnF$_{20}$TPPDL** loaded PLGA NPs incubation without irradiation; (c) irradiation without ***trans*-ZnF$_{20}$TPPDL** loaded PLGA NPs incubation; (d) 60 μg·ml^{-1} ***trans*-ZnF$_{20}$TPPDL** loaded PLGA NPs incubation combined with irradiation.

3. Supporting information for theoretical calculations

3.1 Table S4. The number of the excited state in ascending energy (#), calculated wavelengths (λ_{calc}) and oscillator strengths (f_{calc}), observed wavelengths of the Faraday $\mathcal{B}_0$ terms in the MCD spectra (λ_{obs}), oscillator strengths calculated from the experimental spectra (f_{obs}) through spectral band decovolution with the SIMPFIT program[a] of both spectra with Gaussian-shaped bands, and wavefunctions for **H_2F_{20}TPP**, **H_2F_{20}TPPL**, ***cis*-** and ***trans*-H_2F_{20}TPPDL**, **ZnF_{20}TPP**, **ZnF_{20}TPPL,** and ***cis*-** and ***trans*-ZnF_{20}TPPDL**.

#	λ_{calc}	f_{calc}	λ_{obs}	f_{obs}	Wavefunction =
					H_2F_{20}TPP
1	591	0.00	---	---	52% **s** → **-s**; 48% **a** → **-a**;…
2	535	0.01	---	---	52% **s** → **-a**; 47% **a** → **-s**;…
3	372	1.15	---	---	48% **a** → **-a**; 39% **s** → **-s**; 11% $2b_{1u}$ → -s;…
4	358	1.64	---	---	53% **a** → **-s**; 48% **s** → **-a**;…
					H_2F_{20}TPPL
1	586	0.04	---	---	60% **a** → **-a**; 40% **s** → **-s**;…
2	527	0.02	---	---	50% **s** → **-a**; 40% **a** → **-s**;…
3	366	1.20	---	---	47% **s** → **-s**; 25% **a** → **-a**;…
4	359	1.63	---	---	44% **a** → **-s**; 37% **s** → **-a**; 12% **s** → **-s**;…
					***cis*-H_2F_{20}TPPDL**
1	577	0.12	654	0.06	79% **a** → **-a**; 21% **s** → **-s**;…
2	529	0.01	539	0.00	53% **s** → **-a**; 45% **a** → **-s**;…
3	363	1.67	412	0.53	52% **a** → **-s**; 42% **s** → **-a**;…
4	354	1.39	403	0.56	77% **s** → **-s**; 19% **a** → **-a**;…
					***trans*-H_2F_{20}TPPDL**
1	630	0.15	675	0.09	74% **a** → **-a**; 18% **s** → **-s**; 5% **s** → **-a**;…
2	547	0.06	551	0.02	55% **s** → **-a**; 36% **a** → **-s**; 7% **s** → **-s**;…
3	364	1.61	411	0.83	56% **a** → **-s**; 36% **s** → **-a**;…
4	350	1.53	399	0.55	77% **s** → **-s**; 17% **a** → **-a**;…
					ZnF_{20}TPP
1	538	0.00	---	---	42% **a** → **-a**; 35% **s** → **-s**; 12% **a** → **-s**; 10% **s** → **-a**;…
2	538	0.00	---	---	42% **a** → **-s**; 35% **s** → **-a**; 12% **a** → **-a**;10% **s** → **-s**;…
3	356	1.50	---	---	50% **s** → **-a**; 42% **a** → **-s**;…
4	356	1.50	---	---	50% **s** → **-s**; 43% **a** → **-a**;…
					ZnF_{20}TPPL
1	556	0.09	---	---	76% **a** → **-a**; 23% **s** → **-s**;…
2	514	0.00	---	---	50% **s** → **-a**; 49% **a** → **-s**;…
3	359	1.46	---	---	49% **a** → **-s**; 47% **s** → **-a**;…
4	350	1.33	---	---	75% **s** → **-s**; 44% **a** → **-a**;…
					***cis*-ZnF_{20}TPPDL**
1	557	0.17	632	0.12	87% **a** → **-a**; 12% **s** → **-s**;…
2	525	0.00	574	0.03	51% **s** → **-a**; 47% **a** → **-s**;…
3	366	1.40	430	0.54	46% **a** → **-s**; 45% **s** → **-a**;…
4	343	1.10	418	0.63	86% **s** → **-s**; 13% **a** → **-a**;…
					***trans*-ZnF_{20}TPPDL**
1	624	0.25	667	0.19	89% **a** → **-a**; 11% **s** → **-s**;…
2	538	0.01	606	0.02	55% **s** → **-a**; 43% **a** → **-s**;…
3	363	1.43	426	0.74	54% **a** → **-s**; 40% **s** → **-a**;…
6	336	1.19	408	0.44	87% **s** → **-s**; 9% **a** → **-a**;…

[a] An in house piece of software developed for the analysis of UV-visible absorption and magnetic circular dichroism (MCD) spectra by the research group of Prof. Martin J. Stillman at the University of Western Ontario. Details have been published: Browett, W. R.; Stillman, M. J. *Inorg. Chim. Acta* **1981**, *49*, 69-77, Gasyna, Z.; Browett, W. R.; Nyokong, T.; Kitchenham, R.; Stillman, M. J. *Chemom. Intell. Lab. Syst.* **1989**, *5*, 233-246, Mack, J. Ph.D. Thesis, University of Western Ontario 1994, and Mack, J.; Stillman, M. J. *Coord. Chem Rev.* **2001**, *219-221*, 993-1032.

3.2. The complete reference of Gaussian 09

Gaussian 09, Revision A.02, M. J. Frisch, G. W. Trucks, H. B. Schlegel, G. E. Scuseria, M. A. Robb, J. R. Cheeseman, G. Scalmani, V. Barone, B. Mennucci, G. A. Petersson, H. Nakatsuji, M. Caricato, X. Li, H. P. Hratchian, A. F. Izmaylov, J. Bloino, G. Zheng, J. L. Sonnenberg, M. Hada, M. Ehara, K. Toyota, R. Fukuda, J. Hasegawa, M. Ishida, T. Nakajima, Y. Honda, O. Kitao, H. Nakai, T. Vreven, J. A. Montgomery, Jr., J. E. Peralta, F. Ogliaro, M. Bearpark, J. J. Heyd, E. Brothers, K. N. Kudin, V. N. Staroverov, R. Kobayashi, J. Normand, K. Raghavachari, A. Rendell, J. C. Burant, S. S. Iyengar, J. Tomasi, M. Cossi, N. Rega, J. M. Millam, M. Klene, J. E. Knox, J. B. Cross, V. Bakken, C. Adamo, J. Jaramillo, R. Gomperts, R. E. Stratmann, O. Yazyev, A. J. Austin, R. Cammi, C. Pomelli, J. W. Ochterski, R. L. Martin, K. Morokuma, V. G. Zakrzewski, G. A. Voth, P. Salvador, J. J. Dannenberg, S. Dapprich, A. D. Daniels, Ö. Farkas, J. B. Foresman, J. V. Ortiz, J. Cioslowski, and D. J. Fox, Gaussian, Inc., Wallingford CT, 2009.

4. ^{1}H-, ^{19}F-, ^{13}C-NMR, IR and HR-ESI MS spectra

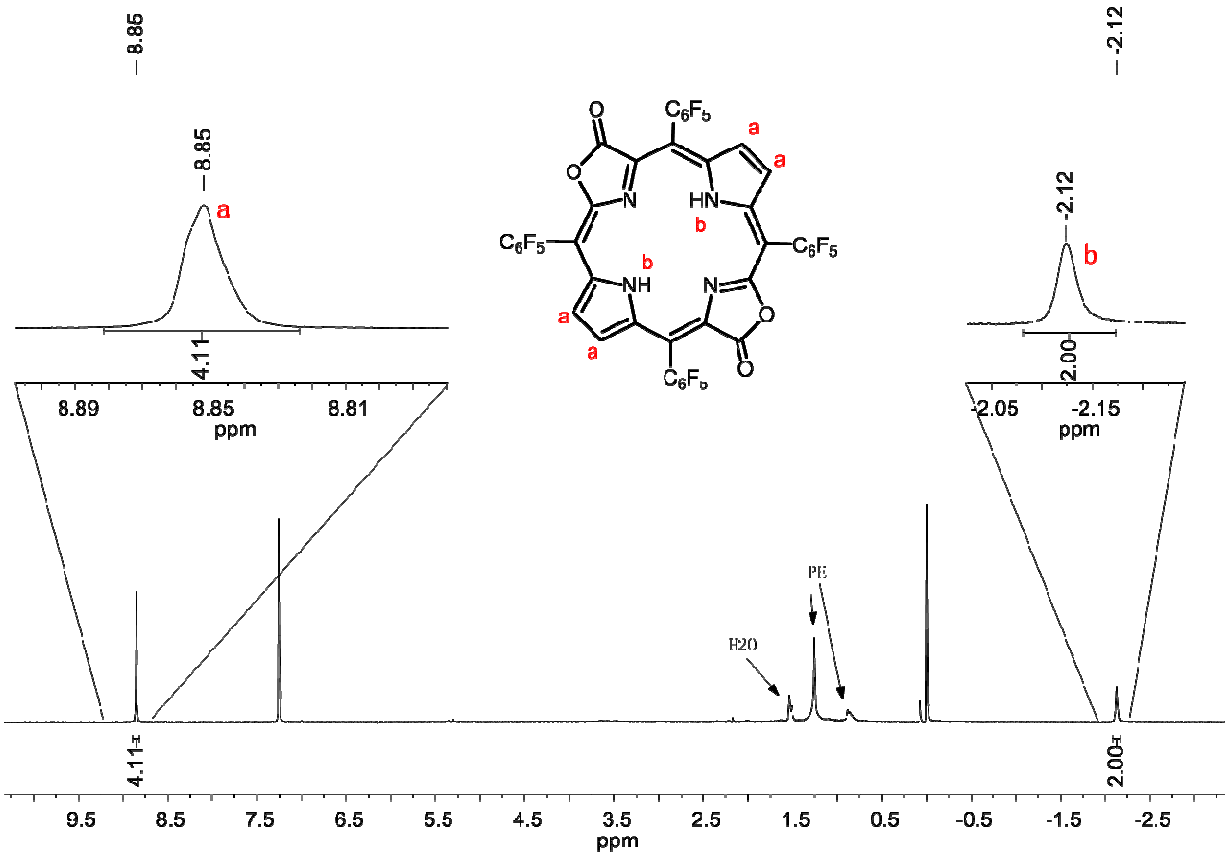

4.1. Figure S19. ^{1}H NMR spectrum of ***trans*-H_2F_{20}TPPDL** in $CDCl_3$.(400MHz)

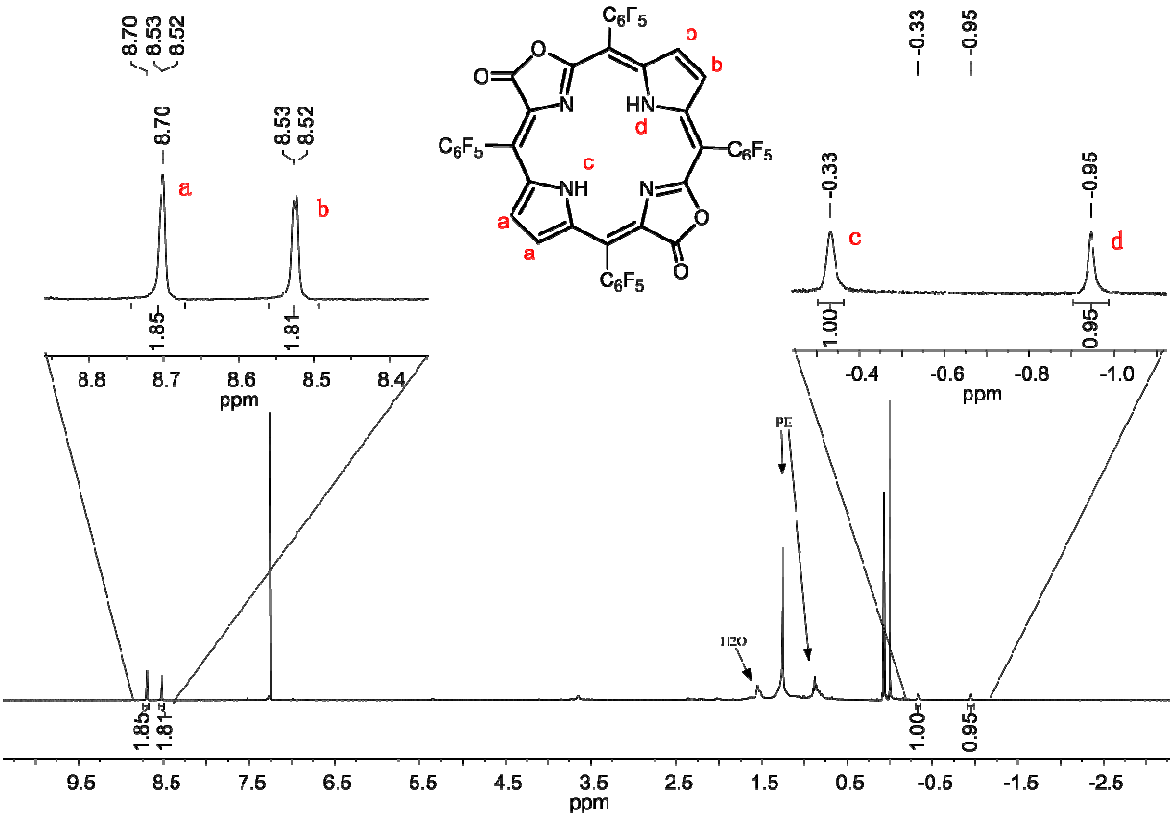

4.2. Figure S20. ^{1}H NMR spectrum of ***cis*-H_2F_{20}TPPDL** in $CDCl_3$. (400MHz)

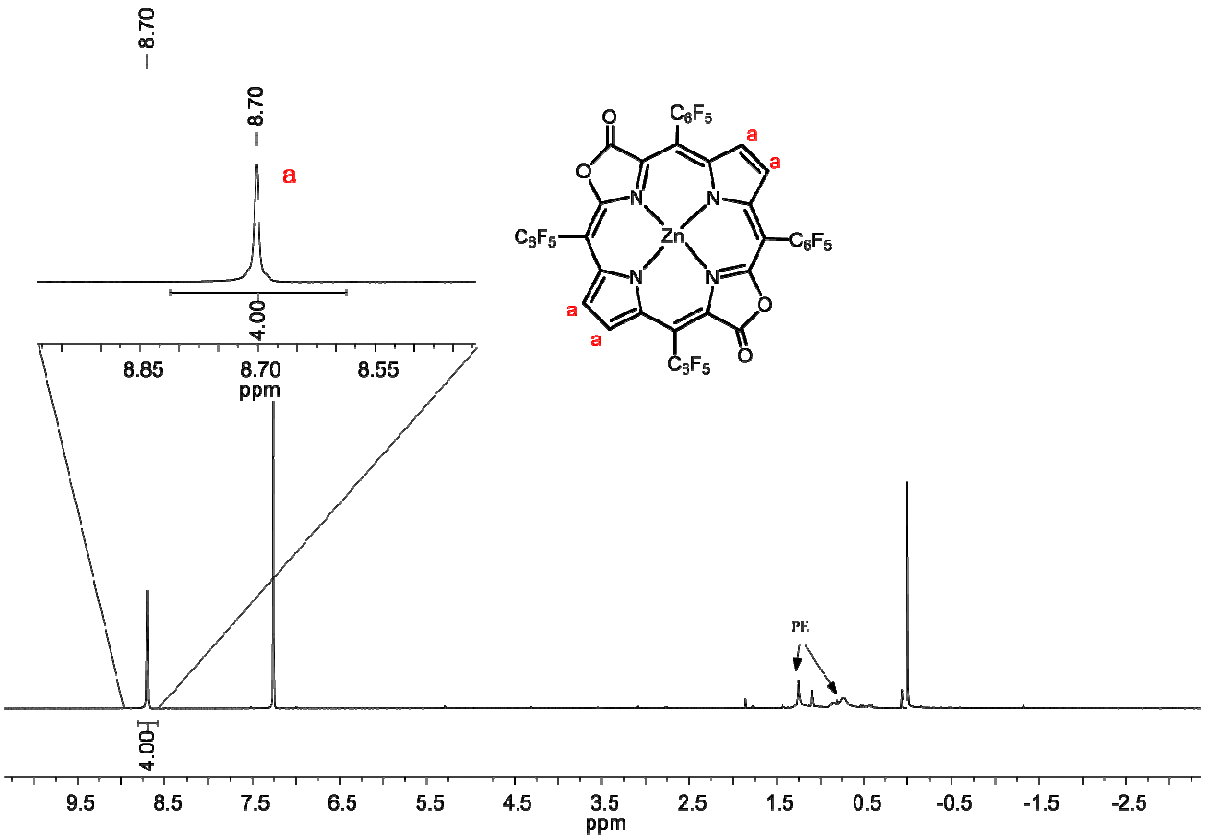

4.3. Figure S21. ^{1}H NMR spectrum of ***trans*-ZnF$_{20}$TPPDL** in $CDCl_3$. (400MHz)

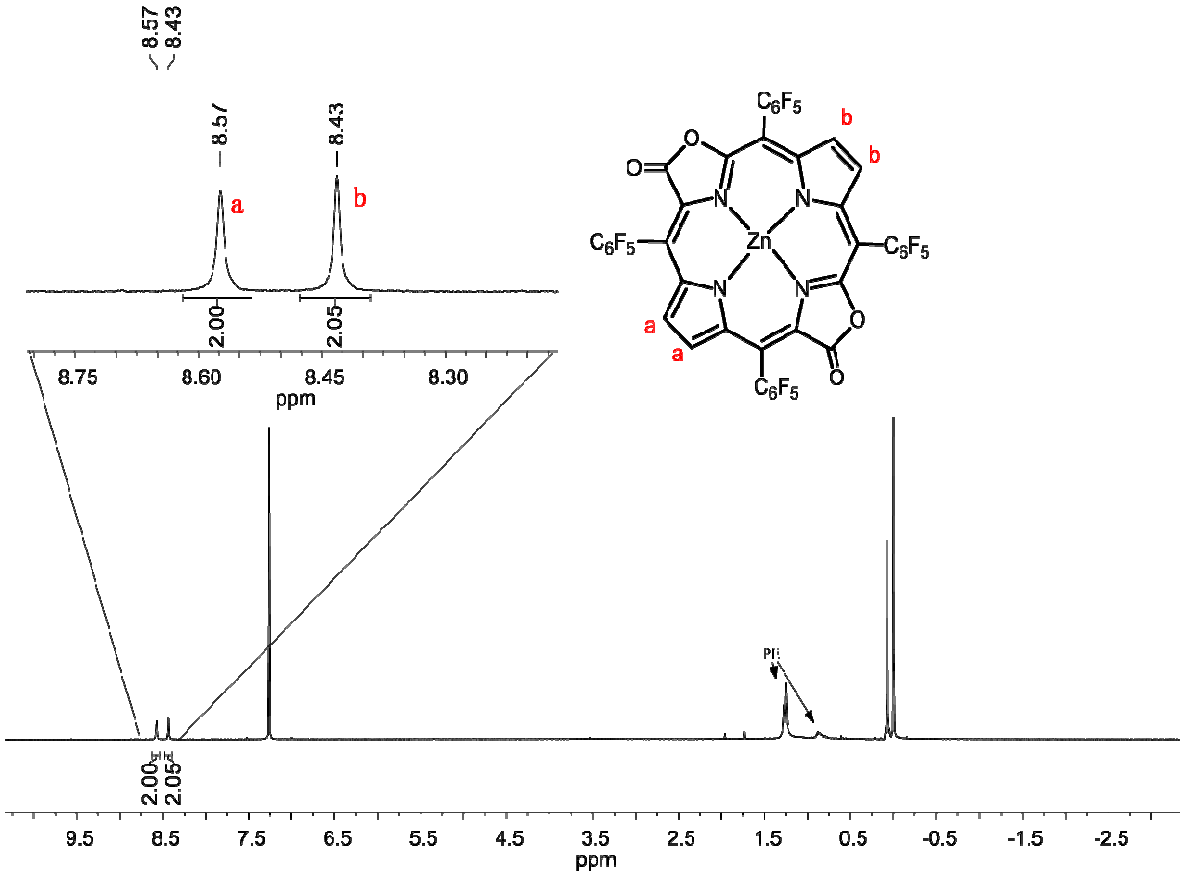

4.4. Figure S22. ^{1}H NMR spectrum of ***cis*-ZnF$_{20}$TPPDL** in $CDCl_3$. (400MHz)

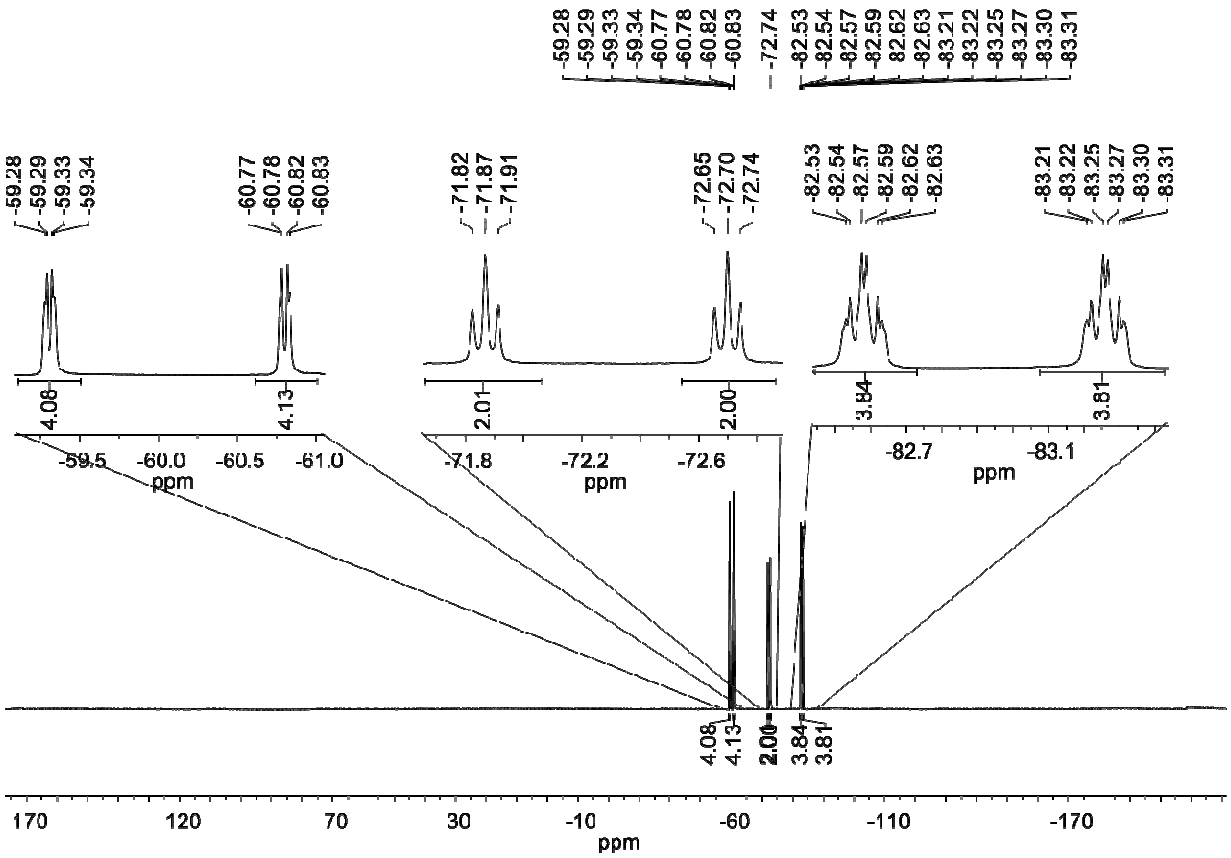

4.5. Figure S23. ^{19}F NMR spectrum of ***trans*-H_2F_{20}TPPDL** in $CDCl_3$. (471MHz)

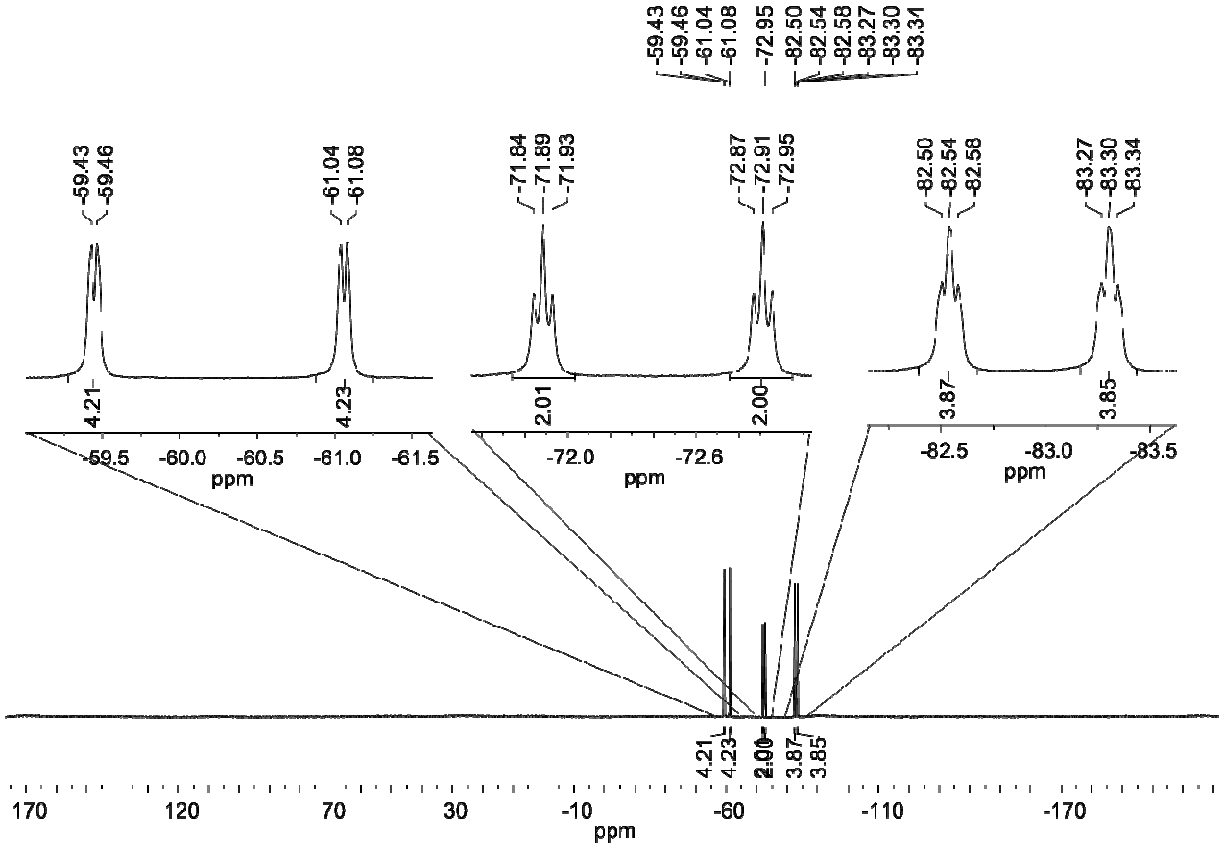

4.6. Figure S24. ^{19}F NMR spectrum of ***cis*-H_2F_{20}TPPDL** in $CDCl_3$. (471MHz)

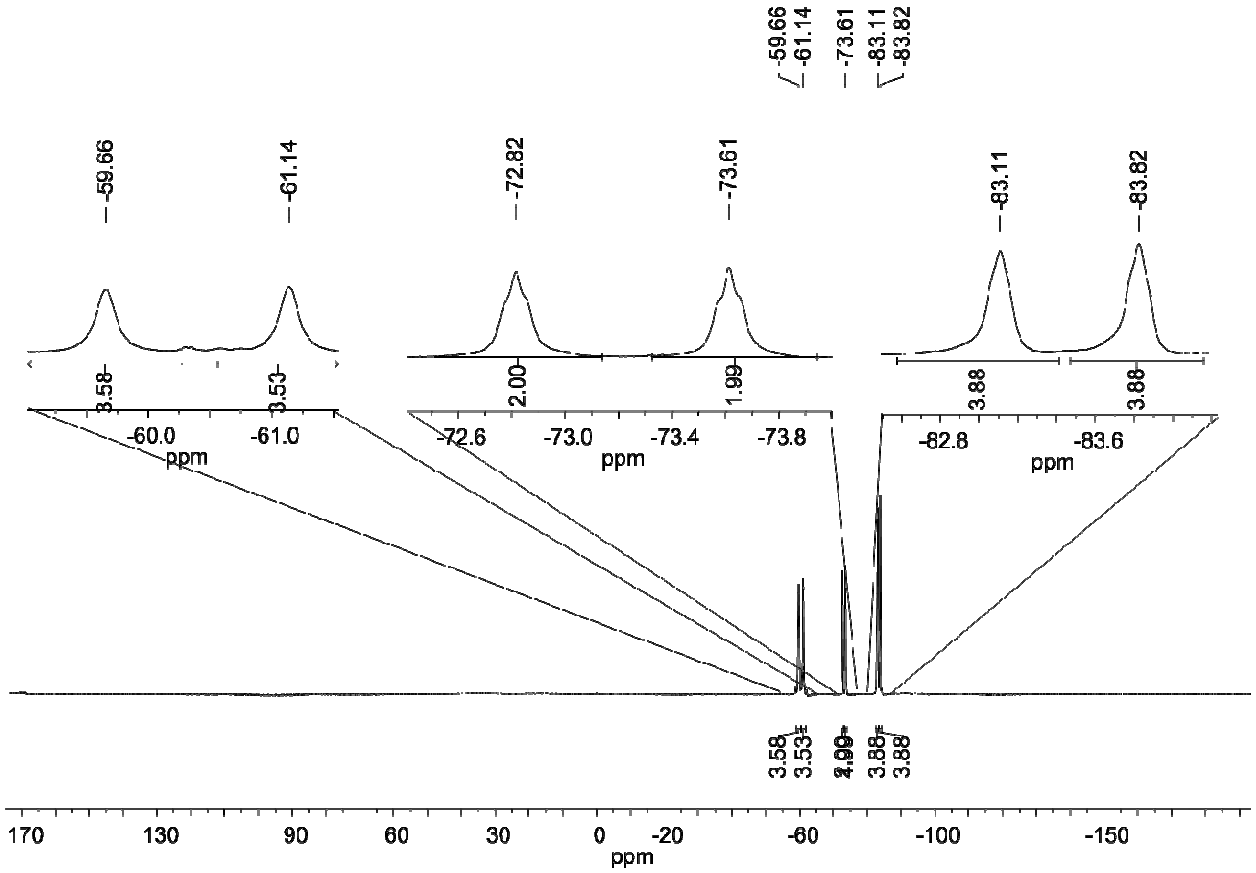

4.7. Figure S25. ^{19}F NMR spectrum of ***trans*-ZnF$_{20}$TPPDL** in $CDCl_3$. (471MHz)

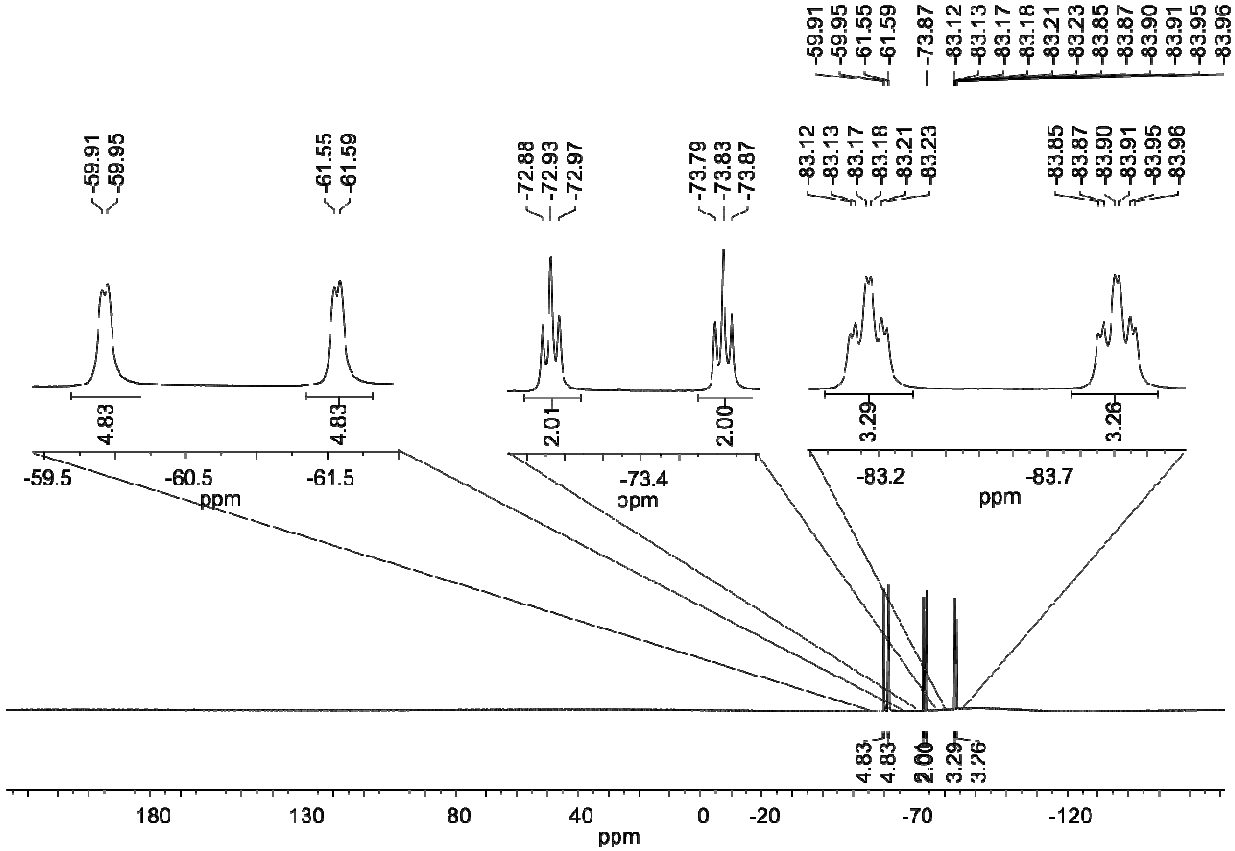

4.8. Figure S26. ^{19}F NMR spectrum of ***cis*-ZnF$_{20}$TPPDL** in $CDCl_3$. (471MHz)

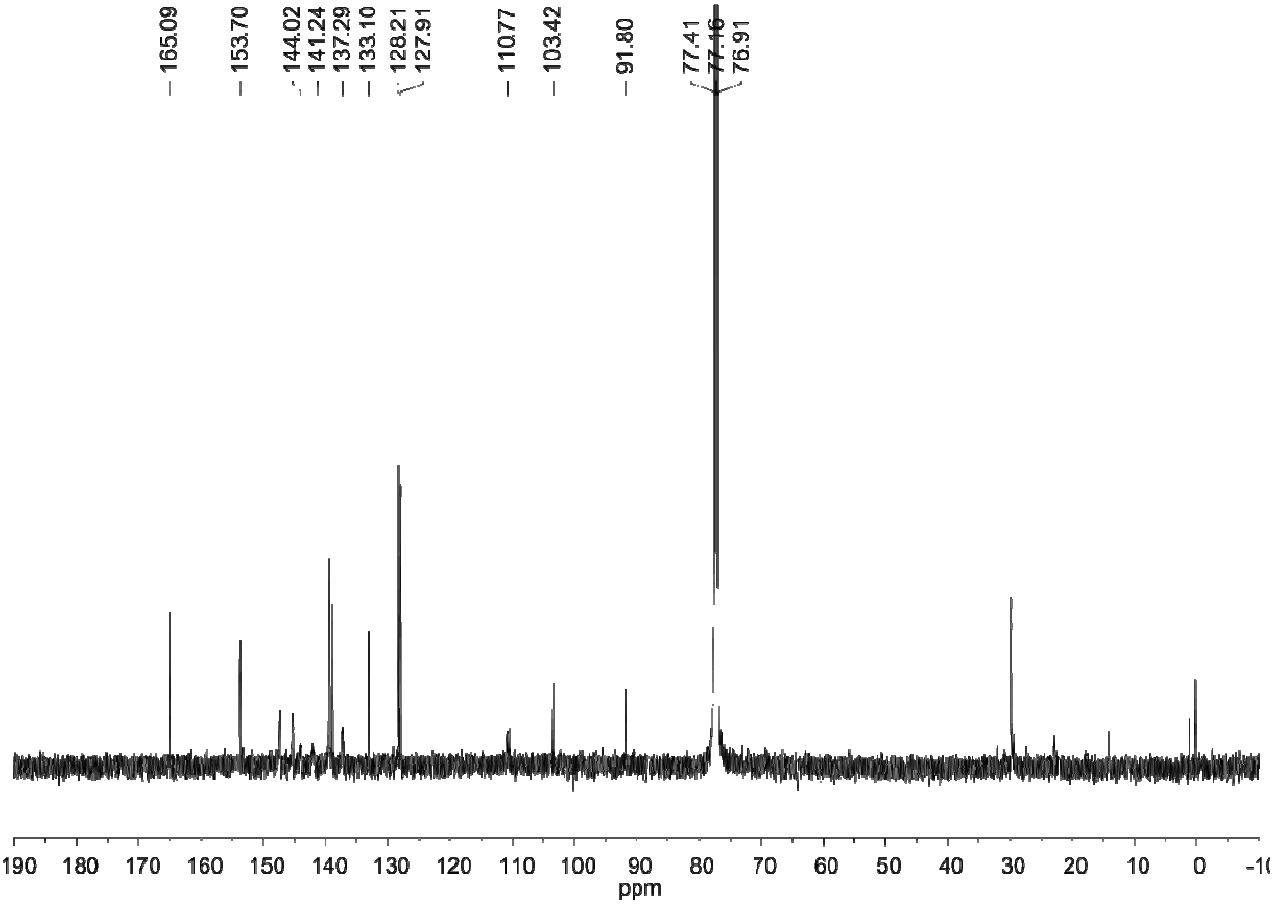

4.9. Figure S27. ^{13}C NMR spectrum of ***trans*-H_2F_{20}TPPDL** in $CDCl_3$. (126MHz)

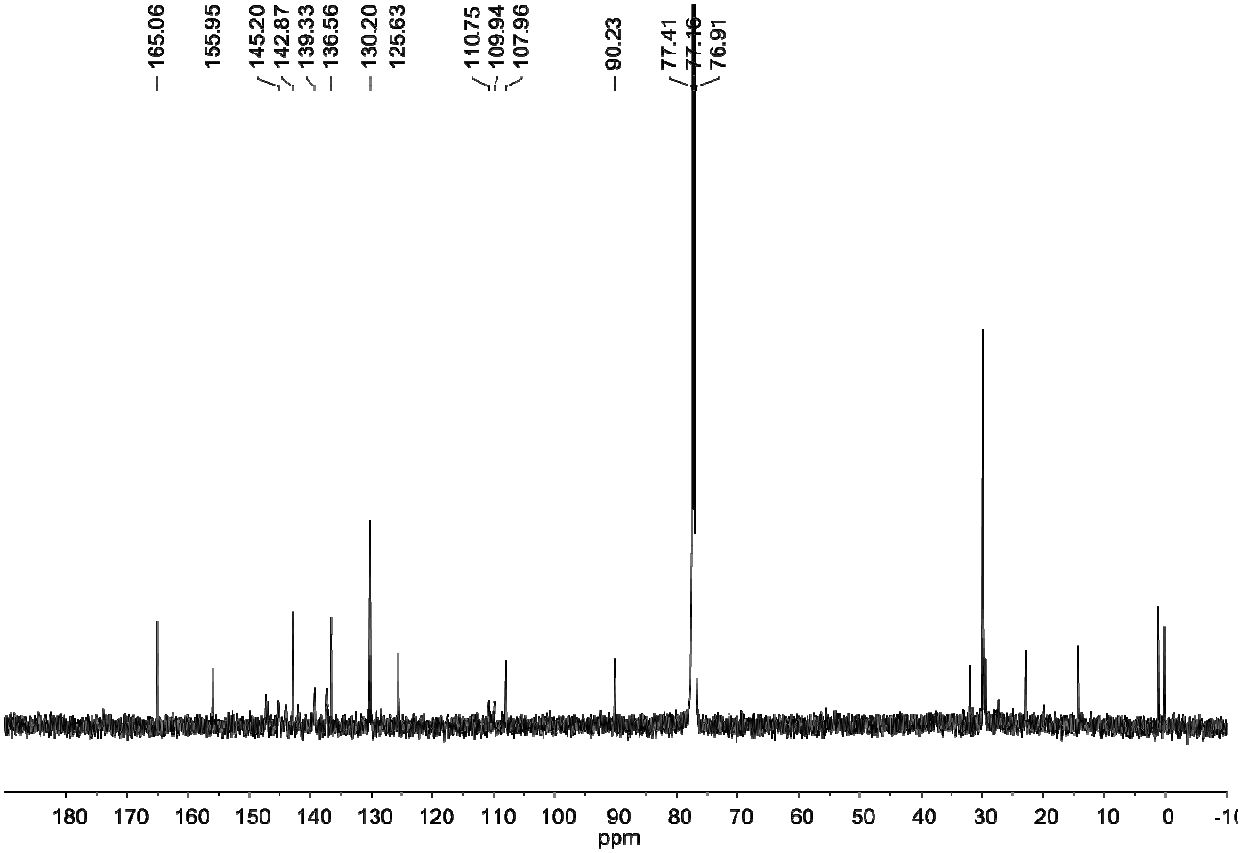

4.10. Figure S28. ^{13}C NMR spectrum of ***cis*-H_2F_{20}TPPDL** in $CDCl_3$. (126MHz)

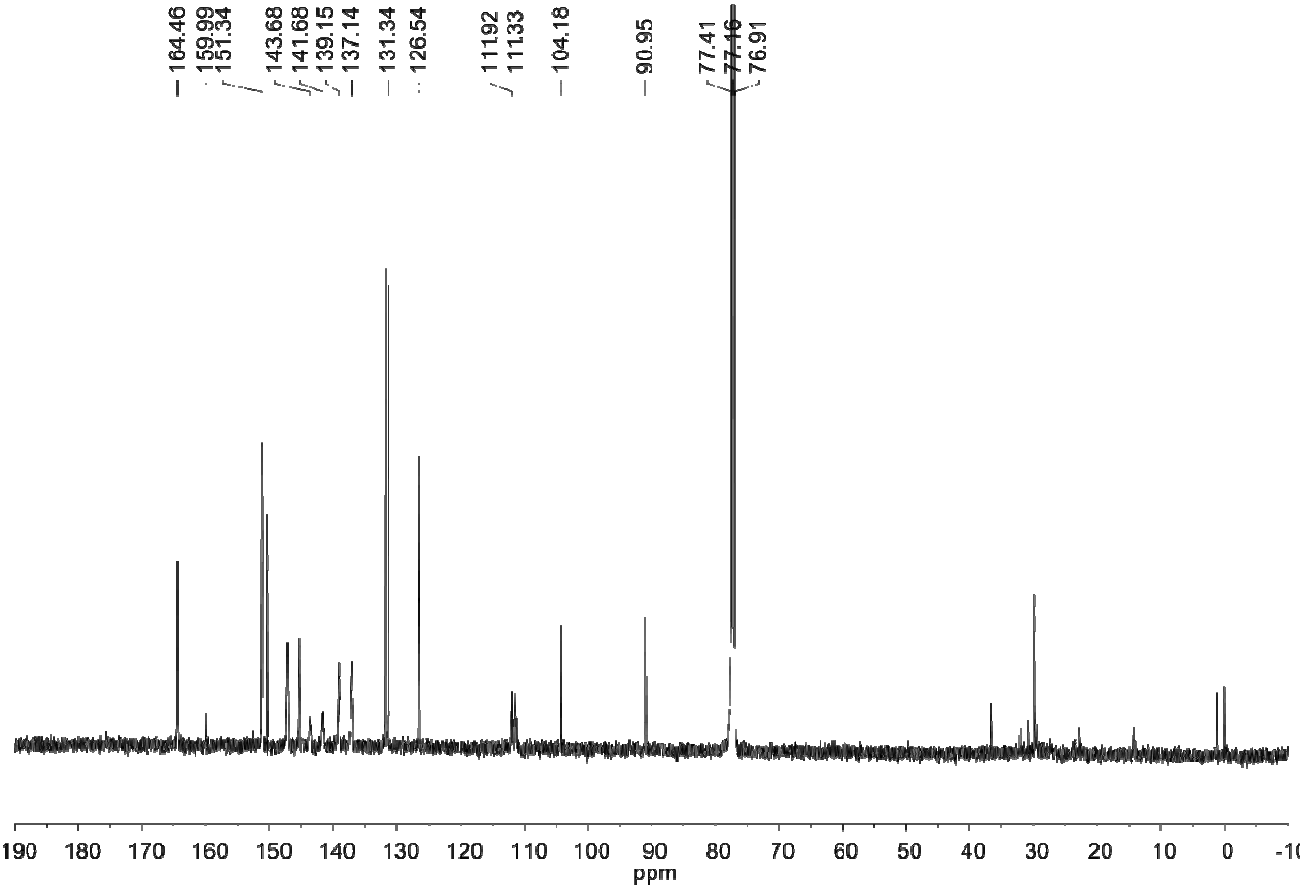

4.11. Figure S29. ^{13}C NMR spectrum of ***trans*-ZnF$_{20}$TPPDL** in $CDCl_3$. (126MHz)

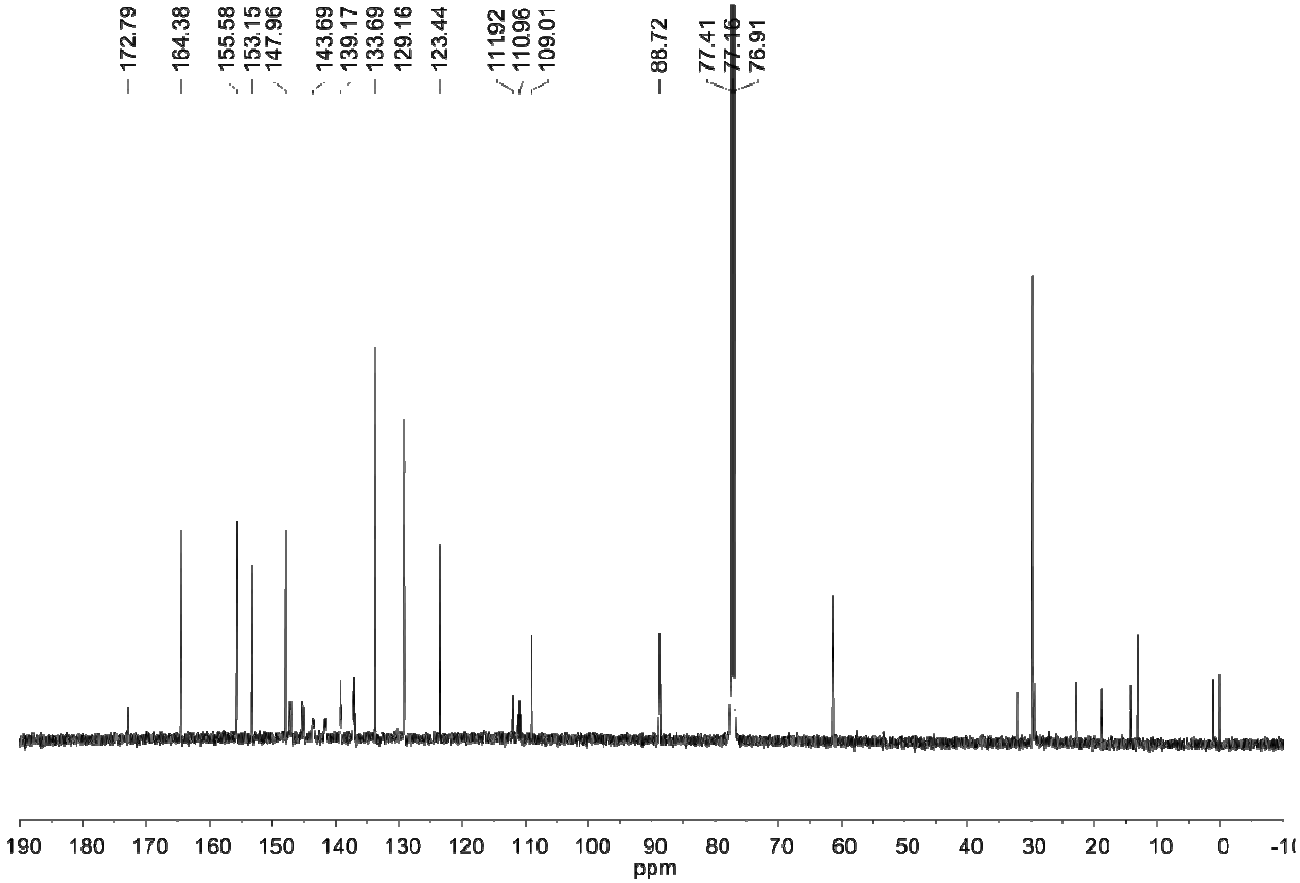

4.12. Figure S30. ^{13}C NMR spectrum of ***cis*-ZnF$_{20}$TPPDL** in $CDCl_3$. (126MHz)

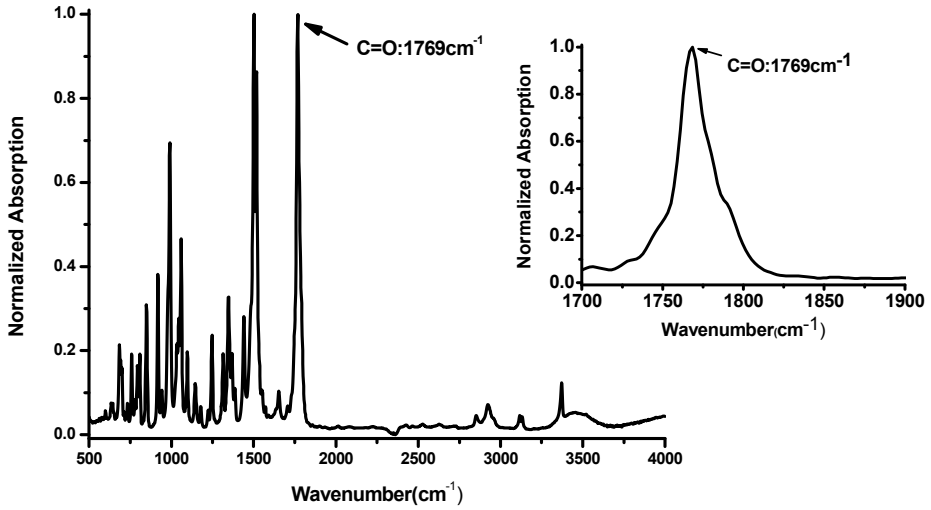

4.13. Figure S31. Normalized FI-IR spectra of ***trans*-H_2F_{20}TPPDL**.

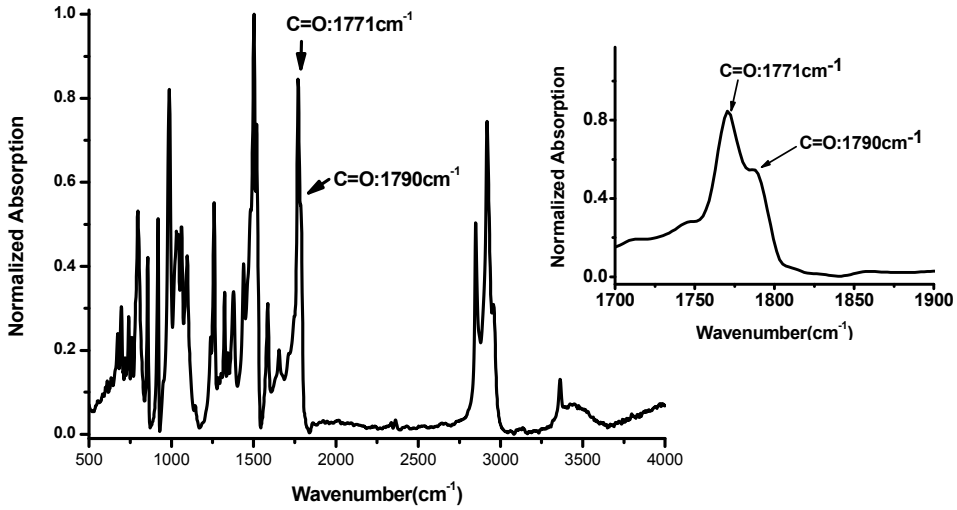

4.14. Figure S32. Normalized FI-IR spectra of ***cis*-H_2F_{20}TPPDL**.

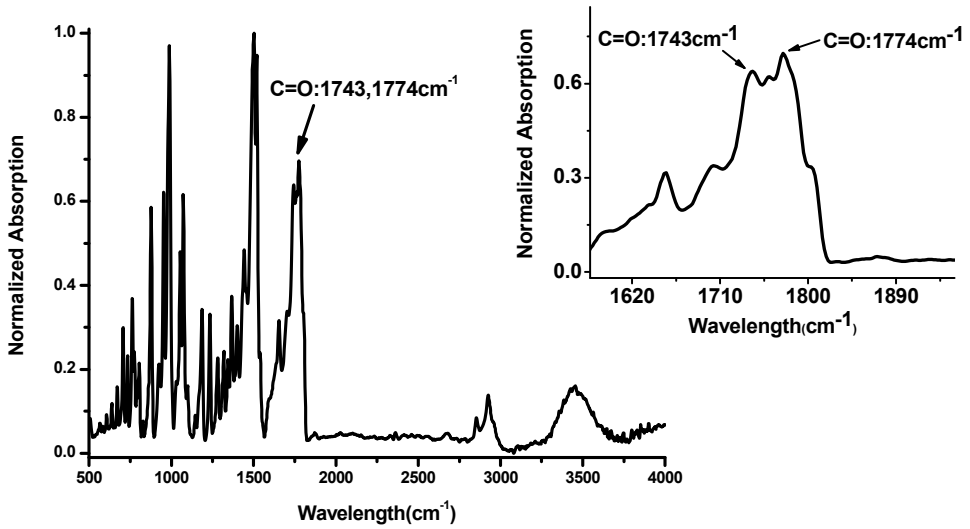

4.15. Figure S33. Normalized FI-IR spectra of ***trans*-ZnF$_{20}$TPPDL**.

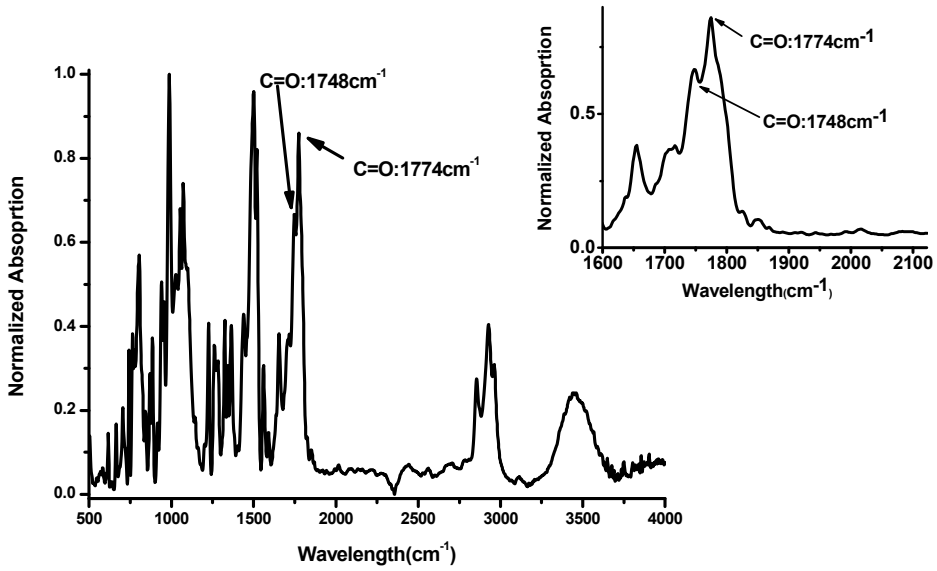

4.16. Figure S34. Normalized FI-IR spectra of ***cis*-ZnF$_{20}$TPPDL**.

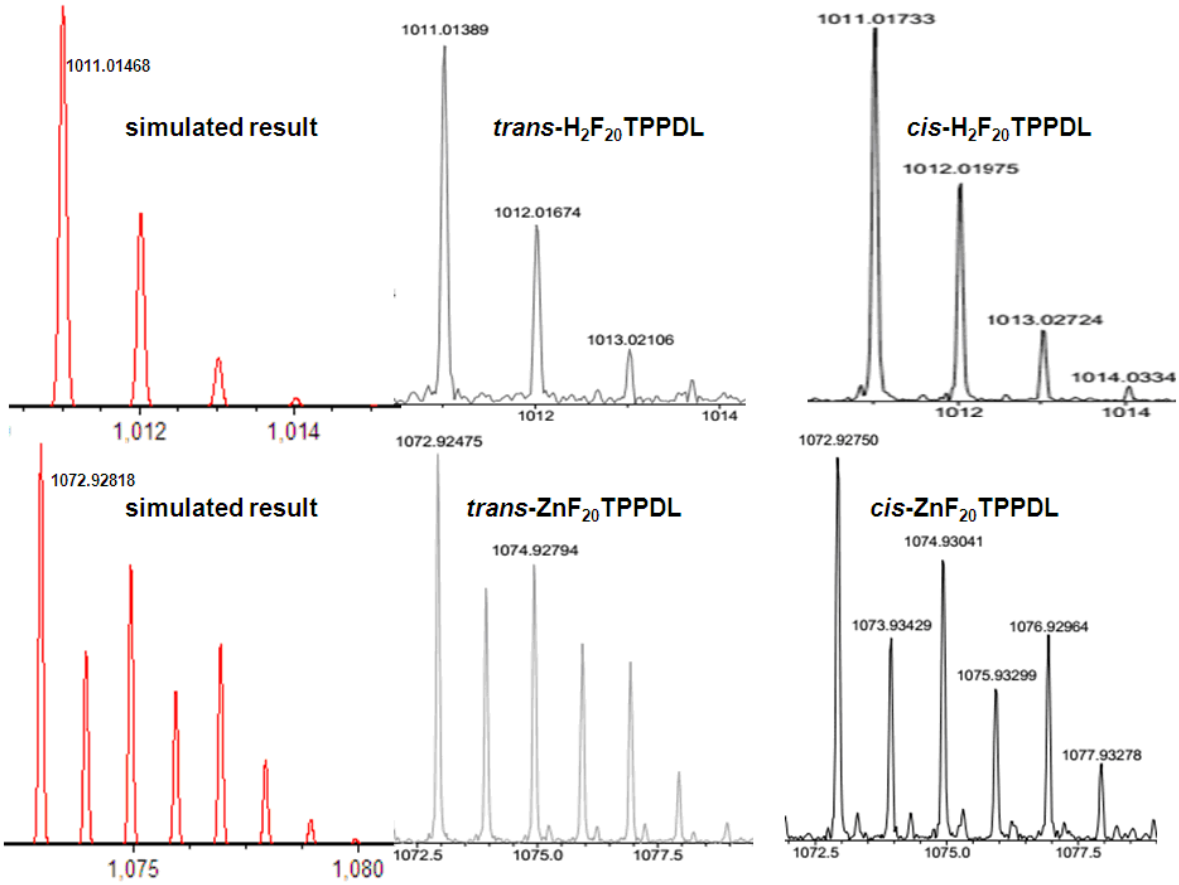

4.17. Figure S35. HR ESI-MS spectra and simulated results of porphodilactones.